Physical Properties, Kinematics, and Substructure in the Molecular Gas of Infrared Dark Clouds

William J. Dirienzo[1], Crystal Brogan[2], Rémy Indebetouw[2,3], Claire J. Chandler[2], Rachel K. Friesen[4], Kathryn E. Devine[5]

[1]University of Wisconsin-Sheboygan, [2]National Radio Astronomy Observatory, [3]University of Virginia, [4]Dunlap Institute for Astronomy and Astrophysics, [5]College of Idaho

Abstract:
Infrared Dark Clouds (IRDCs) harbor the earliest phases of massive star formation, and many of the compact cores in IRDCs, traced by millimeter continuum or by molecular emission in high critical density lines, host massive protostars. We used the Robert C. Byrd Green Bank Telescope (GBT) and the Very Large Array (VLA) to map NH_3 and CCS in nine IRDCs to reveal the temperature, density, and velocity structures and explore chemical evolution in the dense (>10^{22} cm^{-2}) gas. Ammonia is an ideal molecular tracer for these cold, dense environments. The internal structure and kinematics of the IRDCs include velocity gradients, filaments, and possibly colliding sub-clouds that elucidate the formation process of these structures and their protostars. We find a wide variety of substructure including filaments and globules at distinct velocities, sometimes overlapping at sites of ongoing star formation. It appears that these IRDCs are still being assembled from molecular gas clumps even as star formation has already begun, and at least three of them appear consistent with morphology of the "hub-filament structure" discussed in the literature. Furthermore, we find that these clumps are typically near equipartition between gravitational and kinetic energies, so these structures may survive for multiple free-fall times.

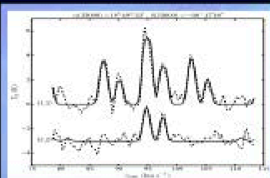

Spectral Line Fitting Routine:
We have written and implemented python code to fit the full hyperfine structure of the ammonia (1,1) and (2,2) inversion lines. The code is capable of handling multiple marginally resolved velocity components along the line of sight in a highly automated way. For each velocity component, the code computes a model spectrum from five free parameters: a central velocity, a velocity width, an optical depth, an excitation temperature, and a rotation temperature. The rotation temperature has been shown to scale well with the kinetic temperature. The inclusion of both the optical depth and excitation temperature allows for an unambiguous determination of the column density, and thus the mass. This information reveals the nature of starless and protostellar cores.

Clump Assignments:
It is readily apparent in the data that regions containing at least two strong, distinct velocity components, if not three or four, are common. Attempts to fit a single velocity component to the NH_3 spectra in these regions result in poor fits with unphysically large linewidths and optical depths, so multiple components must be included. By performing clump deconvolution on the data before fitting, it is trivial to determine the number of components to include at each line of sight. Sophisticated clump deconvolution algorithms make use of the data cube and its noise properties as a whole, and so are more robust determinations of the number of components to fit than any method making this determination on a line of sight (pixel-by-pixel) basis. Additionally, identifying significant, coherent emission in the data allows us to make very good initial estimates of the central velocities and velocity widths at each line of sight for each component by making first- and second-order moment maps (velocity field and velocity dispersion, respectively) restricted to emission within the identified clump. Finally, using these clumps provides a straightforward and physically motivated way to analyze the physical parameter results from the fitting for different substructures within the clouds. We perform clump deconvolution on the NH_3 (1,1) data using the cprops package described by Rosolowsky & Leroy, 2006. We use the main hyperfine component of the (1,1) line because it typically has the highest signal-to-noise ratio and the (2,2) line does not trace the coldest, and often lowest column density, gas.

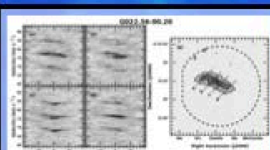

G022.56-00.20 is deconvolved into three subclouds with cprops. The central velocity component (v_{LSR}~77 km s^{-1}) is located at the northeastern end of the cloud, while the high (v_{LSR}~78 km s^{-1}) and low (v_{LSR}~75 km s^{-1}) velocity components have high aspect ratios (A_r~3) and run nearly parallel to each other along the cloud's major axis. The 75 km s^{-1} velocity component is located slightly to the north of the 78 km s^{-1} velocity component, though they overlap spatially, and the cloud shows a high velocity dispersion of about 2 km s^{-1} in the overlap region. It is noteworthy that the peak in integrated intensity, the peak in velocity dispersion, and an infrared point source are all coincident in the center of this overlap region. The position-velocity diagrams taken across the cloud parallel to the minor axis clearly show these major velocity components and their interaction. We identify two possible scenarios for G022.56-00.20: (1) this cloud is a collision of multiple subclouds, apparently triggering the formation of the protostar; or (2) the protostar is driving expansion of the molecular gas around it. The separation between the two primary components is ~3 km s^{-1} and they extend ~1 pc, making either scenario plausible.

Observations & Data:
The combination of total power from single-dish observations along with the high resolution of an interferometer is critical for revealing the structure of filamentary clouds, such as IRDCs. Data from the GBT provide total flux on large spatial scales, which is not measured by our VLA observations. All observing configurations include simultaneous observation of the NH_3 (1,1) and (2,2) inversion lines and the CCS (2_1-1_0) line, with rest frequencies of 23.6945 GHz, 23.72263 GHz, and 22.34403 GHz, respectively. NH_3 (1,1) and (2,2) and CCS (2_1-1_0) emission in our sample of IRDCs was observed with the VLA in D configuration. The GBT data were combined with the VLA data in a two-stage process. First, the VLA data were cleaned in CASA using the GBT cube as a starting model. The resulting cube was then combined with the GBT cube again via feathering in CASA. Feathering two images is a simple way to combine the two data sets, but can be sensitive to the shape of the tapering function and to relative calibration uncertainties. Using a cleaned image that has the single dish data as a starting model, rather than the cleaned VLA image alone, mitigates these effects because the cleaning process can correct any potential issues with the feathered image that might be inconsistent with the interferometric visibilities. Combining the data sets by using a clean model alone, however, is also sensitive to calibration errors and can result in a cube with more total flux than the single dish alone, which is not physical. Feathering these resulting cubes with the single-dish brings the total flux in the final combined images back into agreement with the single-dish data. Interpreting discrete velocity components, velocity gradients, and elevated velocity dispersions as evidence of colliding clumps and/or gas flowing along filaments can be misleading because of the lack of information in the third spatial dimension and the velocities in the plane of the sky. To move forward with understanding the kinematics and the chemistry in IRDCs, we observed G031.97+00.07 in a suite of molecular lines and 3 mm continuum with the Combined Array for Research in Millimeter-wave Astronomy (CARMA). Nine dense gas tracers were observed in G031.97+00.07 with CARMA in D configuration (the second most compact configuration).

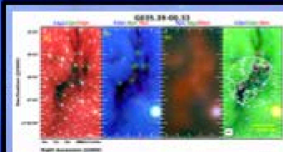

G035.39-00.33 is a long, filamentary, high IR contrast cloud with protostellar candidates. The velocity structure shows two distinct velocity components: a v_{LSR}~45 km s^{-1} velocity subcloud at the northern end of our observations, and a v_{LSR}~45 km s^{-1} velocity filament in the main cloud with a gradient from the southeast to the northwest. The two components are well separated in velocity space, and position-velocity slices do not show any apparent interaction between the two. We see high velocity dispersion around most of the protostars, only one of which is coincident with the lower velocity component. Our GBT data, which cover much more of the cloud and have higher velocity resolution, show that the velocity gradient in the 45 km s^{-1} component continues along the northern extent of the filament. We suggest that this IRDC may also represent an example of the hub-filament structure, in which gas is flowing along the parsec-scale 45 km s^{-1} filament to the region we studied, where it feeds the ongoing star formation traced by infrared point sources.

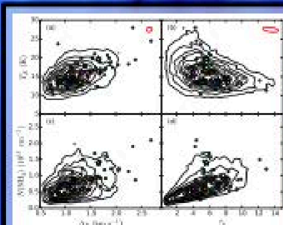

Plots of the results of pixel-by-pixel NH_3 spectral line fitting are shown above, as well as averages over clumps and whole clouds. The velocity FWHM, kinetic temperature, optical depth in the (1,1) line, and column density are generally correlated. G034.43+00.24 (cyan) is notable as having the highest Δv, T_K, and $N(NH_3)$ in the sample, dominated by the emission surrounding the bright protostars with outflows as traced by masers and extended green objects (EGOs; bright 4.5 µm sources often attributed to shocked molecular hydrogen emission in protostellar outflows). G028.23-00.19 is also notable for being apparently starless throughout, and is colder and has a higher τ_1 than the rest of the sample. Most of the clumps have an average NH_3 optical depth τ_1 greater than 3 and all are greater than 1, indicating that these clumps are typically optically thick in NH_3 emission. We see velocity dispersion typically around 2 km s^{-1}, greater than the thermal linewidths, which are typically less than 0.1 km s^{-1}.

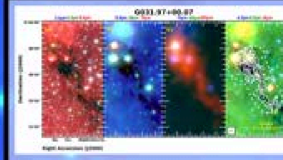

G031.97+00.07 has the most complex substructure in our sample. The cloud itself is part of a much larger molecular complex seen in ^{13}CO in the BU-GRS with infrared dark filaments extending beyond our observations. Seen above, The NH_3 emission closely matches the infrared contrast, and it is deconvolved into 21 distinct clumps. The structures are a mix of filaments and globules, and tend to fall in one of two distinct velocity ranges: v_{LSR}~92-99 km s^{-1} and v_{LSR}~97-102 km s^{-1}. The majority of the emission is in the 92-99 km s^{-1} velocity range, however the 97-102 km s^{-1} velocity range is coincident with at least one protostar. The filamentary structures also show velocity gradients spanning about 2 km s^{-1} along their major axis. This cloud also has the strongest CCS emission in our sample, with a peak signal-to-noise ratio of about 22. G031.97+00.07 may be a region where several weaker filaments extending tens of parsecs are feeding molecular gas and star formation is progressing most quickly at the collision points. The morphology and velocity structure of this cloud is consistent with the "hub-filament structure" described in Myers, 2009 and Li et al., 2013, in which gas flows along the filaments to a central hub where it feeds star formation. Finally, they note the existence of at least three bubbles all seen in Spitzer, Herschel, and the BU-GRS that are likely older H II regions from previous generations of massive stars, and may have compressed the molecular gas to form and/or shape the IRDC and trigger more recent massive star formation.

G034.43+00.24 has a complex substructure. The overall shape is very filamentary, and it is a portion of the Giant Molecular Filament GMF38.1-32.4a identified by Ragan et al., 2014. The cloud is known to have three protostars with masers, EGOs, and millimeter cores along the primary filament, with an additional protostar at the northern end of the cloud. Shown in the below. The velocity dispersion is elevated to over 2 km s^{-1} at two of the protostar positions. There is an overall gradient from the southwest to the northeast. The major filament has a velocity gradient from the west to the east, leading into a gradient from south (v_{LSR}~56 km s^{-1}) to north (v_{LSR}~60 km s^{-1}) along the weaker filament toward the northern protostar. This gradient may be the result of gas flowing along the larger GMF, or may be composed of multiple subclouds not resolved in velocity.

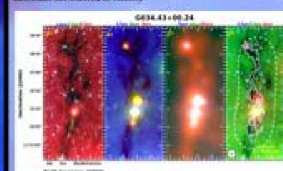

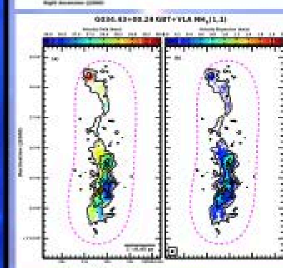

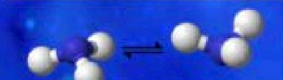

References:

- Ballesteros-Paredes, J., Hartmann, L. W., Vázquez-Semadeni, E., Heitsch, F., & Zamora-Avilés, M. A. 2011, MNRAS, 411, 65
- Busquet, G., Palau, A., Estalella, R., Girart, J. M., Sánchez-Monge, Á., Viti, S., Ho, P. T. P., & Zhang, Q. 2010, A&A, 517, L6
- Li, H. b., Fang, M., Henning, T., & Kainulainen, J. 2013, MNRAS, 436, 3707
- Myers, P. C. 2009, ApJ, 700, 1609
- Ragan, S. E., Henning, T., Tackenberg, J., et al. 2014, A&A, 568, A73
- Rosolowsky, E. & Leroy, A. 2006, PASP, 118, 590

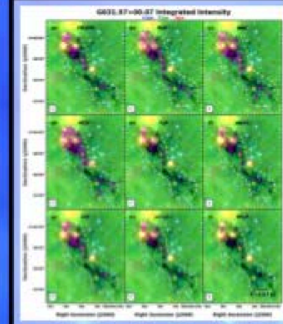

A noteworthy location is the bright IR point source at the far northeastern end of our observations. This point source was beyond the coverage of our VLA NH_3 and CCS observations, however our GBT maps showed the NH_3 (1,1) and (2,2) maxima to be centered on this source (spectra are shown below). The strongest detection of most of the species in this study is located towards this source, except for HNC and N_2H^+, which still have strong detections there, and NH_2D, which was not detected there at all. Both HNC and HCO^+ have profiles consistent with self-absorption towards this source, and the detections of $HN^{13}C$ and $H^{13}CO^+$ provide further evidence that HNC and HCO^+ are optically thick along this line of sight. The nondetection of NH_2D is not surprising given that this source is probably a relatively evolved protostar, and the relative abundance of deuterated ammonia is typically lower in protostellar sources Busquet et al., 2010. We fit the spectra along individual lines of sight in our CARMA data using variations of the method used to fit the NH_3 spectra.

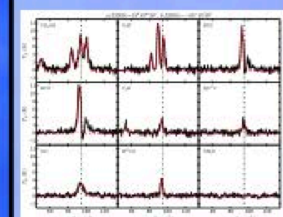

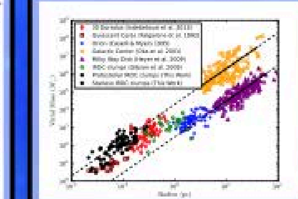

We can place the clumps identified in this study in the context of other molecular gas clumps in varying environments and physical characteristics by putting them on a plot of size versus linewidth or, equivalently, size and spherical virial mass. We additionally use the presence or absence of a 70 µm point source within the boundaries of a clump to classify it as "protostellar" or "starless," respectively. It is notable that the trend seen across different studies between radius and linewidth extends over more than 3 orders of magnitude in size, regardless of the molecular line tracers and observations used. We note that both classes of our clumps are along the same trend, though the Molecular clumps may be virialized but still have higher velocity dispersions (and thus virial masses) than Larson's relation for galactic disk clumps if there exists some external pressure. Elevated linewidths may be a result of chaotic gravitational collapse, in which the turbulent motion arises from the collapse. An alternative explanation is pressure from the gravity of the larger IRDC cloud as a whole. In this sample, we have already shown that the clumps have strong supersonic turbulence, which likely accounts for the relationship between the size and velocity dispersions Ballesteros-Paredes et al., 2011. However, the velocity dispersions being elevated above the typical Milky Way relation requires the clumps to not be in equilibrium (as in the case of outflows), or have additional external pressure beyond that of the warm ISM.